INORGANIC CHEMISTRY FRONTIERS

RESEARCH ARTICLE

View Article Online
View Journal | View Issue

Cite this: *Inorg. Chem. Front.*, 2023, **10**, 1279

Direct CO_2 photoreduction from flue gas by synergistic catalysis of a nickel metal–organic framework and a ruthenium polypyridyl complex†

Man Dong,‡[a] Yu Tian,‡[c] Jian-Xia Gu,[a,d] Xiao-Hui Wang,[a] Lin-Xin Wang,[a] Bao-Shan Hou,[a] Afifa Yousuf,[a] Chun-Yi Sun, *[a] Jie Wu,[e] Zhen-Hui Kang, *[e] Xin-Long Wang *[a] and Zhong-Min Su [b]

Direct photoreduction of CO_2 from flue gas is an energy-saving avenue to realize the carbon-neutral cycle but it is still in its infancy. Herein, we constructed a new anionic metal–organic framework based on trinuclear Ni clusters and thiophenecarboxylic acid for CO_2 photoreduction of exhaust gas from a power plant. Under visible-light irradiation, the yield of CO was 17.4–26.3 mmol g^{-1} in diluted CO_2 with a concentration of 5–20%. The apparent quantum yield (A.Q.Y.) under a 10% CO_2 atmosphere was determined to be 2.1%, which ranks among the highest values of the reported photocatalysts under similar conditions. Importantly, in real flue gas containing 10% CO_2, a selectivity of 90.4% was achieved and CO generation reached 18.2 mmol g^{-1}. *In situ* transient photovoltage (TPV) and density functional theory (DFT) calculations showed that the formation of a CO_2 bridged photocatalytic interface between Ni-MOF1 and a Ru complex ($[Ru(bpy)_3]Cl_2$/$[Ru(bpy)_2]Cl_2$) was a crucial factor for the efficient CO_2-to-CO conversion in diluted CO_2.

Received 8th November 2022,
Accepted 28th December 2022

DOI: 10.1039/d2qi02366k

rsc.li/frontiers-inorganic

1. Introduction

With the gradual increase in the consumption of fossil fuels, the energy crisis and global warming resulting from heavy emission of CO_2 are thorny issues facing human society.[1–4] Reduction of CO_2 into usable carbon-based fuel using solar light has been considered a promising avenue to solve these problems.[5–9] Tremendous efforts have been made in this field and high reaction activity has been achieved but mainly focusing on the utilization of pure CO_2.[10–17] The purification and condensation of low concentration CO_2 [20] utilizing dropwise condensation or supersonic separation technologies[21] is an energy-intensive and complicated process;[22–24] however, the direct usage of CO_2 from the exhaust gas of heavy industries, which contains 3–20% CO_2,[18,19] as the carbon source is an energy-saving, low-cost and sustainable way. However, direct photoreduction of CO_2 from real flue gas is still in its initial stages.

Metal–organic frameworks (MOFs) have attracted tremendous attention in low-concentration CO_2 photoreduction[25–29] due to their advantages of high-density metal nodes and excellent CO_2 adsorption capability.[30–32] Besides, their well-defined crystalline structures can assist in understanding the structure–activity relationship.[33,34] For example, Han *et al.*[35] have demonstrated CO_2 reduction activity of metal–organic monolayers (Ni MOLs) under 10% CO_2 using $[Ru(bpy)_3]Cl_2$ as a photosensitizer. Similarly, Wang and co-workers[36] have reported that Co-based MAF-X27-OH can convert CO_2 into CO with $[Ru(bpy)_3]Cl_2$ as a photosensitizer and the yield from 10% CO_2 is comparable to that from pure CO_2. Although remarkable progress has been achieved towards the practical application of MOFs,[37,38] still the catalytic efficiency at low CO_2 concentration needs to be further improved. Since $[Ru(bpy)_3]Cl_2$ is a commonly used reagent in MOF systems, the development of efficient interface interaction between a MOF, Ru complex, and CO_2 may be significant to enhance the catalytic efficiency,

[a]*Key Laboratory of National & Local United Engineering Laboratory for Power Battery Institution, Northeast Normal University, Changchun, Jilin, 130024, P. R. China. E-mail: suncy009@nenu.edu.cn, wangxl824@nenu.edu.cn*
[b]*State Key Laboratory of Supramolecular Structure and Materials, Institute of Theoretical Chemistry, College of Chemistry, Jilin University, Changchun 130021, China*
[c]*Institute for Interdisciplinary Quantum Information Technology, Jilin Engineering Normal University, Changchun, 130052, P. R. China*
[d]*Department of Chemistry, Xinzhou Teachers University, Xinzhou, 034000, P. R. China*
[e]*Jiangsu Key Laboratory for Carbon-Based Functional Materials & Devices, Institute of Functional Nano & Soft Materials (FUNSOM), Soochow University, Suzhou, Jiangsu, 215123, P. R. China. E-mail: zhkang@suda.edu.cn*

†Electronic supplementary information (ESI) available. CCDC 2061508. For ESI and crystallographic data in CIF or other electronic format see DOI: https://doi.org/10.1039/d2qi02366k

‡These authors contributed equally.

particularly in low-concentration CO_2 reduction.[39] Until now, there has been a lack of profound understanding of the MOF, Ru complex, and CO_2 catalytic interface kinetics and it is still a big challenge to explore such systems.

Herein, a new MOF (Ni-MOF1) with an anionic framework based on thiophenecarboxylic acid and a trinuclear Ni cluster is synthesized for direct CO_2 photoreduction from the flue gas of a power plant. The anionic framework could help to facilitate the collaboration between the MOF and $[Ru(bpy)_3]^{2+}$/$[Ru(bpy)_2]^{2+}$. Under visible-light irradiation, the yield of CO is 17.4–26.3 mmol g^{-1} in diluted CO_2 with a concentration of 5–20%. And the apparent quantum yield (A.Q.Y.) is up to 2.1% which is better than that of most reported MOFs under similar conditions.[11,18] Meanwhile, a selectivity of 90.4% is achieved and the production of CO is up to 18.2 mmol g^{-1} on Ni-MOF1 in flue gas containing 10% CO_2. Mechanistic studies based on DFT calculations and TPV experiments reveal that CO_2 bridged the photocatalytic interface between Ni-MOF1 and the Ru complex in the reduction process, which may account for the relatively high catalytic activity at low concentrations of CO_2.

2. Experimental methods

2.1. Preparation of $(C_2H_6NH_2)^+[Ni_3(\mu_3\text{-}OH)(H_2O)_3(DMTDC)_3](C_2H_5OH)(DMA)_2$ (Ni-MOF1)

$Ni(NO_3)_2{\cdot}6H_2O$ (0.058 g, 0.2 mmol) was added to a mixture of DMA (8 mL) and absolute ethanol (2 mL) containing H_2DMTDC (Shanghai Tensus Bio-tech Co., Ltd) (0.05 g, 0.02 mmol) and KOH (0.0056 g, 0.1 mmol). Then the mixture was placed in a Teflon reactor and heated at 150 °C for 72 h. Brown and long strip crystals were obtained after the reaction system was cooled to room temperature slowly. The product was filtered and washed with DMA. The yield was 82% based on H_2DMTDC. The final empirical formula was determined by combining crystallographic data, and elemental and thermogravimetric analysis data. Elemental analysis calcd: C, 39.33; H, 4.95; N, 3.27. Found: C, 39.21; H, 4.98; N, 3.28. IR data (KBr pellet cm^{-1}): 3286 (w), 3007 (w), 2934 (w), 2858 (w), 2464 (w), 1663 (w), 1614 (m), 1534 (w), 1497 (m), 1420 (w), 1391 (m), 1362 (s), 1334 (m), 1249 (w), 1183 (w), 1012 (m), 969 (w), 895 (w), 797 (w), 768 (m), 678 (w), 652 (w), 598 (w). $(C_2H_6NH_2)^+[Ni_3(\mu_3\text{-}OH)(H_2O)_3(DMTDC)_3](C_2H_5OH)(DMA)_2$ (Ni-MOF1, $DMTDC^{2-}$ = 3,4-dimethylthieno[2,3-*b*]thiophene-2,5-dicarboxylate).

2.2. CO_2 photoreduction

The procedure for photoreduction of CO_2 was carried out in a sealed quartz reactor (50 mL). A circulating cooling water system was used to maintain the reaction temperature at around 20 °C. In a typical reduction reaction, Ni-MOF1 (1 mg), $[Ru(bpy)_3]Cl_2$ (Shanghai Bidepharmatech Co., Ltd) (bpy = 2′,2-bipyridine, 7 mg), water (1 mL), acetonitrile (MeCN, 4 mL) and triethanolamine (TEOA, 1 mL) were placed in a quartz reactor. Then the quartz reactor was filled with a low concentration of CO_2 (CO_2/Ar v/v). The system was irradiated using a 300 W Xe lamp with a cut-off filter (λ > 420 nm). To detect the composition of gas products, 0.5 mL of gas products were sampled and injected into an FID. The yield of CO was calibrated with standard gas mixtures and their identity was determined using their retention time (1.9 min for CO). The injector and detector temperatures were set to 60 °C. To detect the content of H_2, 1 mL of the gas products were injected into a TCD. Subsequently, standard gas mixtures and retention time (0.7 min for H_2) were used to determine the identity and calibrate the yield of H_2.

To explore the source of CO produced by photocatalytic reduction of CO_2, gas chromatography-mass spectrometry (GC-MS) was used to detect the products after an isotopic experiment. In this isotopic experiment, the reaction conditions were the same as described above except that $^{12}CO_2$ was replaced by $^{13}CO_2$.

3. Results and discussion

3.1. Characterization of the structure

Single-crystal X-ray structural analysis revealed that Ni-MOF1 crystallizes in the $P6_3/mmc$ space group. The asymmetric unit consists of one Ni(II) ion, one coordinated water molecule, one third μ_3-OH^-, and one $DMTDC^{2-}$ ligand. Every Ni(II) ion is six-coordinated with four oxygen atoms from four different $DMTDC^{2-}$ ligands, one coordinated water molecule, and one μ_3-OH^-. The structure of the crystal consists of $Ni_3(\mu_3\text{-}OH)$ cores and $DMTDC^{2-}$ ligands, which is similar to the structure of MIL-88B (Fig. 1a).[40] Five $Ni_3(\mu_3\text{-}OH)$ cores and six $DMTDC^{2-}$ ligands form a trigonal bipyramid-type cage (Fig. 1b). From a topological perspective, the whole structure of Ni-MOF1 can be

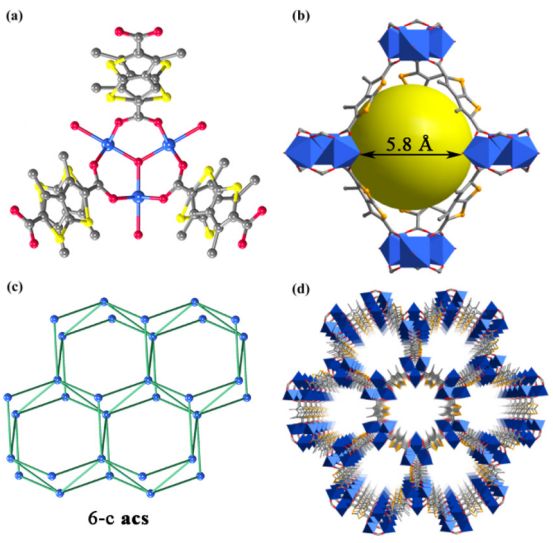

Fig. 1 The structure of Ni-MOF1. (a) The coordination environment of inorganic SBUs. (b) The cage structure. (c) The 6-connected topology network. (d) View of the 3D structures along the *c* axis (blue balls: Ni; red balls: O; yellow balls: S; and grey balls: C).

described as a 6-connected acs network (Fig. 1c). Running along the *c* axis, there are hexagonal honeycomb porous channels with a pore size of about 10.1 Å (Fig. 1d). The infrared (IR) spectrum was used to elucidate the connection between the metal and the ligand in Ni-MOF1 (Fig. 2a). It displays saturated hydrocarbon stretching vibrations at 2934 cm^{-1} and 2858 cm^{-1}, and carbonyl vibration at 1663 cm^{-1}. Meanwhile, the peaks at 1497 cm^{-1} and 1420 cm^{-1} are attributed to the skeletal vibrations of the aromatic ring. The flexural vibrational peak of saturated hydrocarbons is observed at 1391 cm^{-1}. No vibrational peak of the oxygen–hydrogen (hydroxyl) bond in the carboxyl group was observed, indicating that the Ni(II) atom of Ni-MOF1 is coordinated with the carbonyl oxygen of the carboxyl group in the ligand. Powder X-ray diffraction (PXRD) was used to determine the phase purity of Ni-MOF1. A good agreement between peak positions of the simulated prototype and the synthesized material proved the crystallinity and high purity of Ni-MOF1 (Fig. 2b). The difference between them may be due to the various crystal orientations of the powder samples.[41–43]

To investigate the thermal stability of Ni-MOF1, thermogravimetric analysis (TGA) was conducted from 35 °C to 800 °C in N_2 (Fig. 2c). The framework remains intact up to 294 °C, and above that temperature the structure starts to decompose. To understand the light-absorption ability of Ni-MOF1, UV-vis diffuse reflectance was tested. It showed that Ni-MOF1 has broad absorption in the visible light region (380–700 nm) (Fig. 2d).

3.2. CO_2 photoreduction

Considering that the CO_2 concentration in the exhaust emission of the heavy industry sector is between 3 and 20%, the reactivity of Ni-MOF1 in low CO_2 concentration was first investigated by performing reduction reactions in nitrogen diluted CO_2 with 5%, 10%, and 20% CO_2 concentrations under the model conditions of acetonitrile, H_2O, $[Ru(bpy)_3]Cl_2$ and TEOA (Fig. 3a). When 5% CO_2 was used, the CO yield could reach 17.4 mmol g^{-1} while the selectivity was only 72.8% after reacting for three hours, which may be attributed to inadequate CO_2 and the unused reductive sites in the production of H_2. When 10% CO_2 and 20% CO_2 were used, the yields of CO could be increased to 23.1 mmol g^{-1} and 26.3 mmol g^{-1} with the selectivities of 84.3% and 89.2%, respectively. Meanwhile, an apparent quantum yield (A.Q.Y.) of approximately 2.1% at 420 nm and 10% CO_2 concentration was identified, which is higher than the A.Q.Y. of most reported MOFs at the same concentration of CO_2 (Table S2†).[35,36,44,45] To trace the source of the generated CO, an isotopic experiment was performed with $^{13}CO_2$ as the substrate under similar conditions of CO_2 photoreduction and chromatography-mass spectrometry (GC-MS) was used to examine the products. The strong *m*/*z* peak signal at 29 was assigned to ^{13}CO, which clearly indicated that the produced CO originates from photoreduction of CO_2 instead of other species in the reaction system (Fig. S1, ESI†).

To elucidate the effect of each component of the system on CO_2 photoreduction, four sets of control experiments were performed (Fig. 3b). No CO and H_2 production was observed in the presence of Ar, indicating that the products did not come from the degradation of organic matter in the reaction system. In the absence of Ni-MOF1 or $[Ru(bpy)_3]Cl_2$, no CO and H_2 were produced, demonstrating that Ni-MOF1 and $[Ru(bpy)_3]Cl_2$

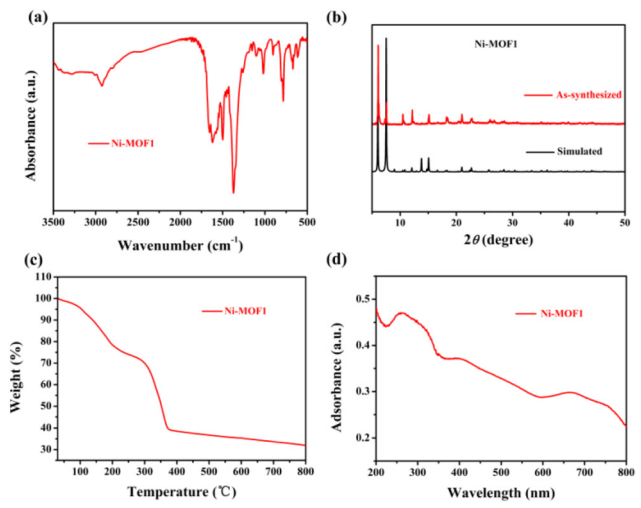

Fig. 2 Basic characterization of Ni-MOF1. (a) Infrared (IR) spectra. (b) Powder X-ray diffraction (PXRD) (black curve: single-crystal simulation and red curve: experimental synthesis). (c) TGA curves. (d) UV-vis diffuse reflectance spectra.

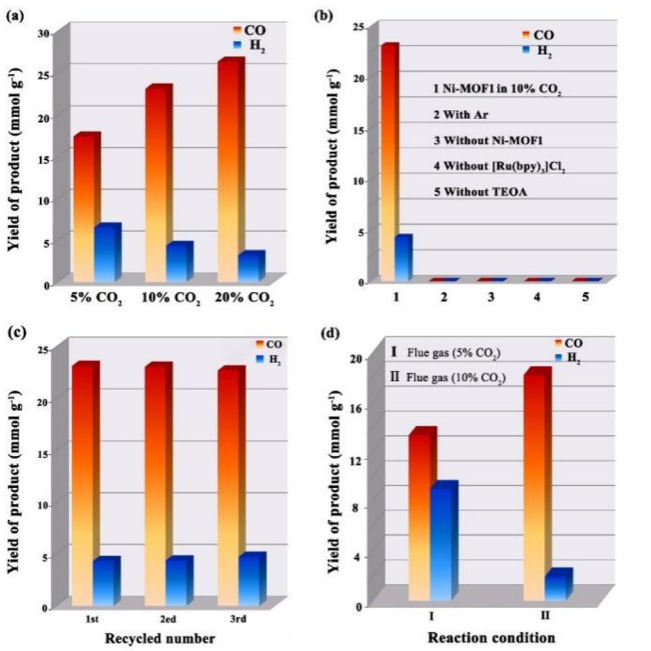

Fig. 3 CO_2 photoreduction performance and recycling. (a) Ni-MOF1 under different CO_2 concentrations. (b) Ni-MOF1 under various reaction conditions. (c) Cycling tests under 3 h of irradiation in a 10% CO_2 atmosphere over Ni-MOF1. (d) The yield of CO and H_2 on Ni-MOF1 in real flue gas.

are indispensable. And no products were detected in the absence of TEOA, indicating that TEOA as a sacrificial reagent is crucial for CO_2 photoreduction. Cycling experiments revealed that the stability of Ni-MOF1 at 10% CO_2 concentration was relatively good although a slight decline of CO production in the third reaction run was observed. The slight decline was probably owing to a little weight loss of Ni-MOF1 when cleaning and transferring (Fig. 3c).

Due to the high catalytic activity of Ni-MOF1 at low CO_2 concentrations, the performance of this system towards photoreduction of CO_2 directly from flue gas (5% and 10% CO_2 concentrations) was investigated. Of note, yields of CO of 13.4 and 18.2 mmol g^{-1} could still be obtained in the flue gas with 5% and 10% CO_2 concentration, respectively (Fig. 3d). Peculiarly, a high selectivity of 90.4% was observed for the proposed catalyst in the flue gas with 10% CO_2 concentration. Comparing the yields of CO in 5% CO_2 (17.4 mmol g^{-1}) and 10% CO_2 (23.1 mmol g^{-1}), the slight decrease in yield may be mainly attributed to the competitive adsorption and negative effect of other components such as H_2S, SO_x and NO_x.[46] These results indicated that Ni-MOF1 showed pretty good catalytic performance even under harsh reaction conditions, which would provide a valuable guideline to design efficient photocatalysts for practical applications of CO_2 photoreduction.

3.3. Possible catalytic mechanism

To reveal the root reason behind the high reactivity of the system, an *in situ* TPV test was carried out in CO_2 and N_2-saturated ACN solutions. As shown in Fig. 4a, c, and d, the curves of CO_2 and N_2 obtained from Ni-MOF1 are almost the same while the intensity of the curves of CO_2 obtained from the Ru complex and Ru complex/Ni-MOF1 is lower than that of N_2. Compared with that in the Ru complex, a higher intensity curve of N_2 (Fig. 4b) was identified in Ru complex/Ni-MOF1. The above results show that the Ni-MOF1/Ru complex is preponderant in the generation of photoelectrons and is more favorable as an active center for CO_2 photoreduction. For the Ru complex and Ru complex/Ni-MOF1, the equalization $(Q_0 - Q_1)/Q_1$ (the ratio of used number of electrons in CO_2 reduction to the total number of photogenerated electrons) was calculated to be 66.83% and 74.37% (Fig. 4c and d), respectively. A slightly lower value for Ru complex/Ni-MOF1 (66.83%) than that for the Ru complex reveals that the bare Ru complex has a faster reaction rate for CO_2 reduction.

Furthermore, a detailed analysis of the relaxation process using the TPV curves of Ru complex/Ni-MOF1 and Ru complex was conducted. According to the normalized curves of N_2 and CO_2 (Fig. 4e and f), the τ value, representing the time for electron and hole recombination, is also calculated. The τ of the Ru complex under N_2 conditions (0.07511 ms) is larger than that under CO_2 conditions (0.06191 ms) (Fig. 4e). This suggests that the Ru complex can transfer electrons directly to CO_2 for the next reaction step. However, the τ of Ru complex/Ni-MOF1 under N_2 conditions (0.07328 ms) is smaller than that under CO_2 conditions (0.11277 ms) (Fig. 4f). These results indicate that a new photoelectric interface is generated in the CO_2/Ru complex/Ni-MOF1 system. In other words, there is a new CO_2 bridged photocatalytic interface between Ni-MOF1 and the Ru complex. Notably, this kind of CO_2 bridged photocatalytic interface shows a less conductive characteristic than the Ru complex/Ni-MOF1 catalytic interface, but the CO_2 bridged nature is beneficial for the photoreduction of low-concentration CO_2. According to the reported study,[47] the interface has some storage capacity for charge, and therefore it slows down the rate of electron-charge transport. A slower electron transfer process will ensure that the photoexcited charge on

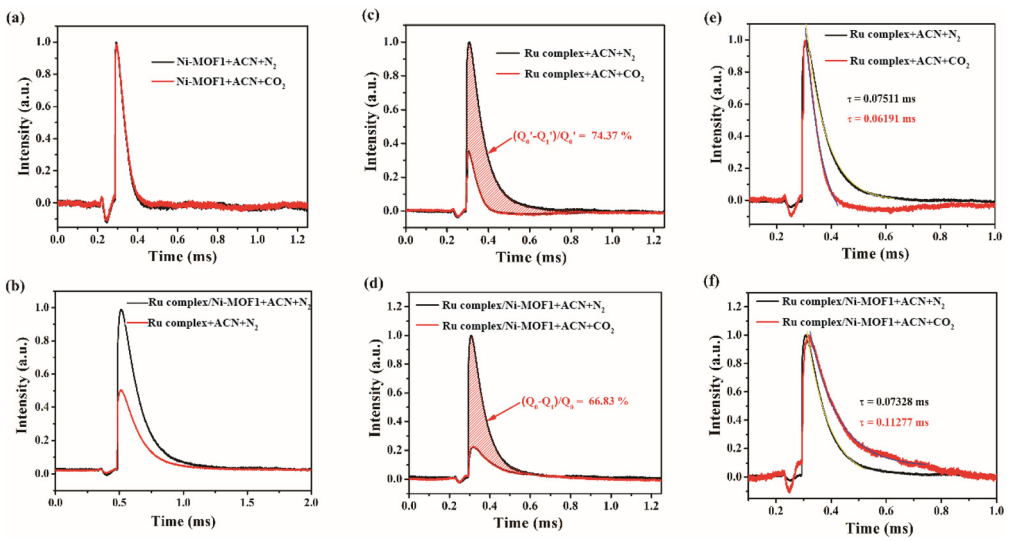

Fig. 4 The *in situ* TPV patterns of different materials in N_2-saturated ACN solution (black curve) and CO_2-saturated ACN solution (red curve). (a) Ni-MOF1. (b) Ru complex/Ni-MOF1 (black curve) and Ru complex (red curve) in N_2-saturated ACN solution. (c) Ru complex. (d) Ru complex/Ni-MOF1. Charge annihilation process of (e) the Ru complex and (f) Ru complex/Ni-MOF1.

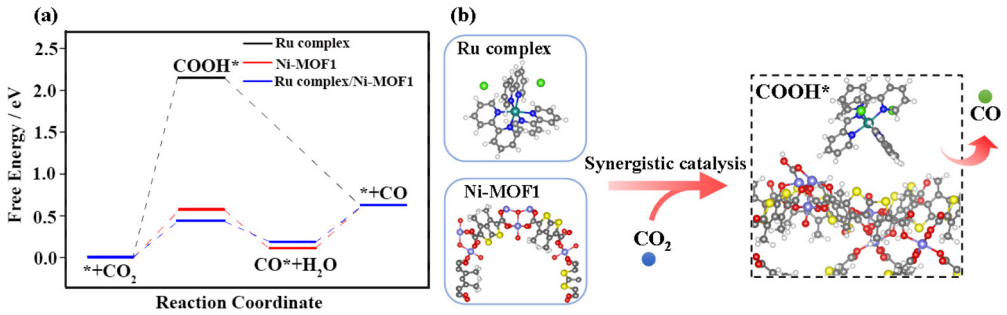

Fig. 5 The DFT results and possible mechanism. (a) Free energy profile for the CO_2RR on Ni-MOF1 and Ru complex/Ni-MOF1 (the free energy zero is set as that of a CO_2 molecule in the gas phase and the catalyst). (b) Synergistic effect of a CO_2 bridged photocatalytic interface of the Ru complex and Ni-MOF1.

the sample surface is maintained for a longer period of time. The extended lifetime of the electrons is an important factor in facilitating the photocatalytic process.

Density functional theory (DFT) calculations were performed to further understand the reaction mechanism of CO_2 reduction to CO. In combination with the results of TPV, the free energy changes (ΔG) on the sites of bare Ni-MOF1, the Ru complex and the CO_2 bridged interface of Ru complex/Ni-MOF1 for CO_2 reduction was calculated. A key step in the reported mechanism is the activation of the classically inert CO_2. In our calculations, ΔG values of COOH* formation on the Ru complex, bare Ni-MOF1 and the Ru complex/Ni-MOF1 interface were 2.15, 0.57 and 0.44 eV, respectively, indicating that the COOH* formed on the Ru complex/Ni-MOF1 interface is more stable (Fig. 5a). In the subsequent step, COOH* will be hydrogenated to CO* by reacting with another proton–electron pair. The ΔG for COOH* hydrogenation to form CO* + H_2O is −0.46 and −0.25 eV, respectively. Besides, due to the weak adsorption of CO on the Ru complex, CO can directly desorb from the substrate with a ΔG of −1.52 eV. The final step is the CO desorption from Ni-MOF1 and the Ru complex/Ni-MOF1 interface after overcoming the larger thermodynamic barrier. Compared with bare Ni-MOF1 as catalyst sites, the synergistic catalytic process of the Ru complex and Ni-MOF1 results in lower energy (ΔG_{max} = 0.44 eV) and more stable intermediates. Thus the CO_2 photoreduction is prone to occur on the CO_2 bridged Ru complex/Ni-MOF1 interface (Fig. 5b). The high catalytic yield at low CO_2 concentrations may be ascribed to this synergistic catalytic process.

4. Conclusions

In summary, a new kind of anionic MOF (Ni-MOF1) based on a trinuclear nickel cluster and $DMTDC^{2-}$ ligand was constructed for direct CO_2 photoreduction from flue gas. Under visible light, a CO yield of 23.1 mmol g^{-1} and an A.Q.Y. of 2.1% were achieved with the assistance of the Ru complex in diluted CO_2 with a concentration of 10%. The A.Q.Y. obtained in this work is comparable to the highest values of all reported photocatalysts under similar conditions. More importantly, in the flue gas containing 10% CO_2 concentration, CO generation was still 18.2 mmol g^{-1} with a selectivity of 90.4%. TPV experiments and DFT calculations indicated that the synergistic catalysis of a CO_2 bridged photocatalytic interface of the Ru complex and Ni-MOF1 played an important role in CO_2 photoreduction, which might be the reason for the high reactivity in low concentration of CO_2. This work provides new insights not only for the construction of a catalytic interface in CO_2 photoreduction but also for the development of efficient photocatalysts for CO_2 reduction directly from flue gas.

Author contributions

M. D. and Y. T. contributed equally to this paper. M. D. and C. Y. S. conceived the ideas. M. D. and X. H. W. designed the experiments, synthesized the sample, measured the photocatalytic performance and wrote the paper. L. X. W. assisted in performing photocatalysis experiments. Y. T. was responsible for the theoretical calculation part. B. S. H. was responsible for crystal analysis. J. W. was responsible for TPV analysis. A. Y. was responsible for article polishing. C. Y. S. and Z. H. K. supervised the project, analyzed the data and revised the paper. J. X. G. helped analyze data and modified the article. X. L. W. and Z. M. S. supervised the project and analyzed the data.

Conflicts of interest

There are no conflicts to declare.

Acknowledgements

This research was made possible as a result of a generous grant from the National Natural Science Foundation of China (21971032 and 22175033) and the Education Department of Jilin Province (JJKH20221153KJ).

References

1 H. Dong, X. Zhang, Y. Lu, Y. Yang, Y.-P. Zhang, H.-L. Tang, F.-M. Zhang, Z.-D. Yang, X. Sun and Y. Feng, Regulation of metal ions in smart metal-cluster nodes of metal-organic frameworks with open metal sites for improved photocatalytic CO_2 reduction reaction, *Appl. Catal., B*, 2020, **276**, 119173–119195.

2 X. Chen, Q. Li, M. Zhang, J. Li, S. Cai, J. Chen and H. Jia, MOF-Templated Preparation of Highly Dispersed Co/Al_2O_3 Composite as the Photothermal Catalyst with High Solar-to-Fuel Efficiency for CO_2 Methanation, *ACS Appl. Mater. Interfaces*, 2020, **12**, 39304–39317.

3 X. Qi, R. Zhong, M. Chen, C. Sun, S. You, J. Gu, G. Shan, D. Cui, X. Wang and Z. Su, Single Metal–Organic Cage Decorated with an Ir(III) Complex for CO_2 Photoreduction, *ACS Catal.*, 2021, **11**, 7241–7248.

4 X. Yu, C.-C. Zhao, J.-X. Gu, C.-Y. Sun, H.-Y. Zheng, L.-K. Yan, M. Sun, X.-L. Wang and Z.-M. Su, Transition-Metal-Modified Vanadoborate Clusters as Stable and Efficient Photocatalysts for CO_2 Reduction, *Inorg. Chem.*, 2021, **60**, 7364–7371.

5 Z. Chen, Y. Hu, J. Wang, Q. Shen, Y. Zhang, C. Ding, Y. Bai, G. Jiang, Z. Li and N. Gaponik, Boosting Photocatalytic CO_2 Reduction on $CsPbBr_3$ Perovskite Nanocrystals by Immobilizing Metal Complexes, *Chem. Mater.*, 2020, **32**, 1517–1525.

6 F. Guo, S. Yang, Y. Liu, P. Wang, J. Huang and W.-Y. Sun, Size Engineering of Metal–Organic Framework MIL-101 (Cr)–Ag Hybrids for Photocatalytic CO_2 Reduction, *ACS Catal.*, 2019, **9**, 8464–8470.

7 X. Deng, J. Albero, L. Xu, H. García and Z. Li, Construction of a Stable Ru–Re Hybrid System Based on Multifunctional MOF-253 for Efficient Photocatalytic CO_2 Reduction, *Inorg. Chem.*, 2018, **57**, 8276–8286.

8 W. Zhu, C. Zhang, Q. Li, L. Xiong, R. Chen, X. Wan, Z. Wang, W. Chen, Z. Deng and Y. Peng, Selective reduction of CO_2 by conductive MOF nanosheets as an efficient co-catalyst under visible light illumination, *Appl. Catal., B*, 2018, **238**, 339–345.

9 I. I. Alkhatib, C. Garlisi, M. Pagliaro, K. Al-Ali and G. Palmisano, Metal-organic frameworks for photocatalytic CO_2 reduction under visible radiation: A review of strategies and applications, *Catal. Today*, 2020, **340**, 209–224.

10 M. Lu, J. Liu, Q. Li, M. Zhang, M. Liu, J.-L. Wang, D.-Q. Yuan and Y.-Q. Lan, Rational Design of Crystalline Covalent Organic Frameworks for Efficient CO_2 Photoreduction with H_2O, *Angew. Chem., Int. Ed.*, 2019, **58**, 12392–12397.

11 A. Crake, K. C. Christoforidis, A. Gregg, B. Moss, A. Kafizas and C. Petit, The Effect of Materials Architecture in TiO_2/MOF Composites on CO_2 Photoreduction and Charge Transfer, *Small*, 2019, **15**, 1805473–1805484.

12 X.-Y. Dao, J.-H. Guo, Y.-P. Wei, F. Guo, Y. Liu and W.-Y. Sun, Solvent-Free Photoreduction of CO_2 to CO Catalyzed by Fe-MOFs with Superior Selectivity, *Inorg. Chem.*, 2019, **58**, 8517–8524.

13 C. Gao, Q. Meng, K. Zhao, H. Yin, D. Wang, J. Guo, S. Zhao, L. Chang, M. He, Q. Li, H. Zhao, X. Huang, Y. Gao and Z. Tang, Co_3O_4 Hexagonal Platelets with Controllable Facets Enabling Highly Efficient Visible-Light Photocatalytic Reduction of CO_2, *Adv. Mater.*, 2016, **28**, 6485–6490.

14 M. Liu, Y.-F. Mu, S. Yao, S. Guo, X.-W. Guo, Z.-M. Zhang and T.-B. Lu, Photosensitizing single-site metal–organic framework enabling visible-light-driven CO_2 reduction for syngas production, *Appl. Catal., B*, 2019, **245**, 496–501.

15 H.-Q. Xu, J. Hu, D. Wang, Z. Li, Q. Zhang, Y. Luo, S.-H. Yu and H.-L. Jiang, Visible-Light Photoreduction of CO_2 in a Metal–Organic Framework: Boosting Electron–Hole Separation via Electron Trap States, *J. Am. Chem. Soc.*, 2015, **137**, 13440–13443.

16 D. Li, M. Kassymova, X. Cai, S.-Q. Zang and H.-L. Jiang, Photocatalytic CO_2 reduction over metal-organic framework-based materials, *Coord. Chem. Rev.*, 2020, **412**, 213262.

17 J. Li, H. Huang, W. Xue, K. Sun, X. Song, C. Wu, L. Nie, Y. Li, C. Liu, Y. Pan, H.-L. Jiang, D. Mei and C. Zhong, Self-adaptive dual-metal-site pairs in metal-organic frameworks for selective CO_2 photoreduction to CH_4, *Nat. Catal.*, 2021, **4**, 719–729.

18 G. V. Last and M. T. Schmick, A review of major non-power-related carbon dioxide stream compositions, *Environ. Earth Sci.*, 2015, **74**, 1189–1198.

19 A. Goeppert, M. Czaun, J.-P. Jones, G. K. Surya Prakash and G. A. Olah, Recycling of carbon dioxide to methanol and derived products–closing the loop, *Chem. Soc. Rev.*, 2014, **43**, 7995–8048.

20 P.-Q. Liao, X.-W. Chen, S.-Y. Liu, X.-Y. Li, Y.-T. Xu, M. Tang, Z. Rui, H. Ji, J.-P. Zhang and X.-M. Chen, Putting an ultra-high concentration of amine groups into a metal–organic framework for CO_2 capture at low pressures, *Chem. Sci.*, 2016, **7**, 6528–6533.

21 W. Sun, X. Cao, W. Yang and X. Jin, Numerical simulation of CO_2 condensation process from CH_4-CO_2 binary gas mixture in supersonic nozzles, *Sep. Purif. Technol.*, 2017, **188**, 238–249.

22 G. Jiang, Q. Huang, S. D. Kenarsari, X. Hu, A. G. Russell, M. Fan and X. Shen, A new mesoporous amine-TiO_2 based pre-combustion CO_2 capture technology, *Appl. Energy*, 2015, **147**, 214–223.

23 A. Hart and N. Gnanendran, Cryogenic CO_2 capture in natural gas, *Energy Procedia*, 2009, **1**, 697–706.

24 A. L. Khan, X. Li, A. Ilyas, M. T. Raza and I. F. J. Vankelecom, Novel sulfonated and fluorinated PEEK membranes for CO_2 separation, *Sep. Purif. Technol.*, 2016, **167**, 1–5.

25 J.-D. Xiao and H.-L. Jiang, Metal–Organic Frameworks for Photocatalysis and Photothermal Catalysis, *Acc. Chem. Res.*, 2019, **52**, 356–366.

26 R. Li, W. Zhang and K. Zhou, Metal–Organic-Framework-Based Catalysts for Photoreduction of CO_2, *Adv. Mater.*, 2018, **30**, 1705512–1705542.
27 A. Dhakshinamoorthy, A. M. Asiri and H. García, Metal–Organic Framework (MOF) Compounds: Photocatalysts for Redox Reactions and Solar Fuel Production, *Angew. Chem., Int. Ed.*, 2016, **55**, 5414–5445.
28 X. Feng, Y. Pi, Y. Song, C. Brzezinski, Z. Xu, Z. Li and W. Lin, Metal–Organic Frameworks Significantly Enhance Photocatalytic Hydrogen Evolution and CO_2 Reduction with Earth-Abundant Copper Photosensitizers, *J. Am. Chem. Soc.*, 2020, **142**, 690–695.
29 S. N. Habisreutinger, L. Schmidt-Mende and J. K. Stolarczyk, Photocatalytic Reduction of CO_2 on TiO_2 and Other Semiconductors, *Angew. Chem., Int. Ed.*, 2013, **52**, 7372–7408.
30 T. Kajiwara, M. Fujii, M. Tsujimoto, K. Kobayashi, M. Higuchi, K. Tanaka and S. Kitagawa, Photochemical Reduction of Low Concentrations of CO_2 in a Porous Coordination Polymer with a Ruthenium(II)–CO Complex, *Angew. Chem., Int. Ed.*, 2016, **55**, 2697–2700.
31 D. Wang, R. Huang, W. Liu, D. Sun and Z. Li, Fe-Based MOFs for Photocatalytic CO_2 Reduction: Role of Coordination Unsaturated Sites and Dual Excitation Pathways, *ACS Catal.*, 2014, **4**, 4254–4260.
32 H.-X. Zhang, Q.-L. Hong, J. Li, F. Wang, X. Huang, S. Chen, W. Tu, D. Yu, R. Xu, T. Zhou and J. Zhang, Isolated Square-Planar Copper Center in Boron Imidazolate Nanocages for Photocatalytic Reduction of CO_2 to CO, *Angew. Chem., Int. Ed.*, 2019, **58**, 11752–11756.
33 W. Yang, H.-J. Wang, R.-R. Liu, J.-W. Wang, C. Zhang, C. Li, D.-C. Zhong and T.-B. Lu, Tailoring Crystal Facets of Metal–Organic Layers to Enhance Photocatalytic Activity for CO_2 Reduction, *Angew. Chem., Int. Ed.*, 2021, **60**, 409–414.
34 B. Hou, C. Qin, C. Sun, X. Wang and Z. Su, Stepwise Construction of Multivariate Metal–Organic Frameworks from a Predesigned Zr_{16} Cluster, *CCS Chem.*, 2021, **3**, 287–293.
35 B. Han, X. Ou, Z. Deng, Y. Song, C. Tian, H. Deng, Y.-J. Xu and Z. Lin, Nickel Metal–Organic Framework Monolayers for Photoreduction of Diluted CO_2: Metal-Node-Dependent Activity and Selectivity, *Angew. Chem., Int. Ed.*, 2018, **57**, 16811–16815.
36 Y. Wang, N.-Y. Huang, J.-Q. Shen, P.-Q. Liao, X.-M. Chen and J.-P. Zhang, Hydroxide Ligands Cooperate with Catalytic Centers in Metal–Organic Frameworks for Efficient Photocatalytic CO_2 Reduction, *J. Am. Chem. Soc.*, 2018, **140**, 38–41.
37 M. Dong, J.-X. Gu, C.-Y. Sun, X.-L. Wang and Z.-M. Su, Photocatalytic reduction of low-concentration CO_2 by metal–organic frameworks, *Chem. Commun.*, 2022, **58**, 10114–10126.
38 H. Fei, M. D. Sampson, Y. Lee, C. P. Kubiak and S. M. Cohen, Photocatalytic CO_2 Reduction to Formate Using a Mn(I) Molecular Catalyst in a Robust Metal–Organic Framework, *Inorg. Chem.*, 2015, **54**, 6821–6828.
39 J. Qin, S. Wang and X. Wang, Visible-light reduction CO_2 with dodecahedral zeolitic imidazolate framework ZIF-67 as an efficient co-catalyst, *Appl. Catal., B*, 2017, **209**, 476–482.
40 H. H. Thorp, Bond valence sum analysis of metal-ligand bond lengths in metalloenzymes and model complexes, *Inorg. Chem.*, 1992, **31**, 1585–1588.
41 B. Han, J. Song, S. Liang, W. Chen, H. Deng, X. Ou, Y.-J. Xu and Z. Lin, Hierarchical $NiCo_2O_4$ hollow nanocages for photoreduction of diluted CO_2: Adsorption and active sites engineering, *Appl. Catal., B*, 2020, **260**, 118208.
42 Y. Jiang, J. Sun, X. Yang, J. Shen, Y. Fu, Y. Fan, J. Xu and L. Wang, Cd-MOF@PVDF Mixed-Matrix Membrane with Good Catalytic Activity and Recyclability for the Production of Benzimidazole and Amino Acid Derivatives, *Inorg. Chem.*, 2021, **60**, 2087–2096.
43 Y. Jiang, J. Song, Z. Xiu, L. Huang, F. Gao, S. Jiao and Y. Bi, Solvent-free syntheses of two pcu topological indium phosphite-oxalates with a novel butterfly motif and proton conductivity, *Microporous Mesoporous Mater.*, 2019, **289**, 109643.
44 T.-T. Zhang, G. Li and X.-B. Cui, Three New Polyoxoniobates Functioning as Different Oxidation Catalysts, *Cryst. Growth Des.*, 2021, **21**, 3191–3201.
45 W. Zhong, R. Sa, L. Li, Y. He, L. Li, J. Bi, Z. Zhuang, Y. Yu and Z. Zou, A Covalent Organic Framework Bearing Single Ni Sites as a Synergistic Photocatalyst for Selective Photoreduction of CO_2 to CO, *J. Am. Chem. Soc.*, 2019, **141**, 7615–7621.
46 S.-H. Guo, X.-J. Qi, H.-M. Zhou, J. Zhou, X.-H. Wang, M. Dong, X. Zhao, C.-Y. Sun, X.-L. Wang and Z.-M. Su, A bimetallic-MOF catalyst for efficient CO_2 photoreduction from simulated flue gas to value-added formate, *J. Mater. Chem. A*, 2020, **8**, 11712–11718.
47 M. Dong, J. Zhou, J. Zhong, H. T. Li, C. Y. Sun, Y. D. Han, J. N. Kou, Z. H. Kang, X. L. Wang and Z. M. Su, CO_2 Dominated Bifunctional Catalytic Sites for Efficient Industrial Exhaust Conversion, *Adv. Funct. Mater.*, 2021, 2110136.